HOKKAIDO UNIVERSITY

Title	Improved Thermal Stability of Efficient Proton-Conducting Anodic ZrO2-WO3 Nanofilms by Incorporation of Silicon Species
Author(s)	Ye, Ke; Aoki, Yoshitaka; Tsuji, Etsushi; Nagata, Shinji; Habazaki, Hiroki
Citation	Journal of The Electrochemical Society, 158(11), C385-C390 https://doi.org/10.1149/2.068111jes
Issue Date	2011-10-05
Doc URL	http://hdl.handle.net/2115/47407
Rights	© The Electrochemical Society, Inc. 2011. All rights reserved. Except as provided under U.S. copyright law, this work may not be reproduced, resold, distributed, or modified without the express permission of The Electrochemical Society (ECS). The archival version of this work was published in J. Electrochem.Soc., 158(11), C385-C390, (2011)
Type	article
File Information	JES158_385-390.pdf

Instructions for use

Hokkaido University Collection of Scholarly and Academic Papers : HUSCAP

Journal of The Electrochemical Society, **158** (11) C385-C390 (2011)
0013-4651/2011/158(11)/C385/6/$28.00 © The Electrochemical Society

Improved Thermal Stability of Efficient Proton-Conducting Anodic ZrO_2-WO_3 Nanofilms by Incorporation of Silicon Species

Ke Ye,[a] Yoshitaka Aoki,[a,b] Etsushi Tsuji,[a,b] Shinji Nagata,[c] and Hiroki Habazaki[a,b,*,z]

[a]*Graduate School of Chemical Sciences and Engineering, and* [b]*Faculty of Engineering, Hokkaido University, Sapporo, Hokkaido, 060-8628, Japan*
[c]*Institute for Materials Research, Tohoku University, Sendai 980-8577, Japan*

Novel proton-conducting amorphous anodic ZrO_2-WO_3-SiO_2 films, 200 nm thick, are prepared by anodizing of sputter-deposited $Zr_{37}W_{47}Si_{16}$ at 100 V with current decay for 1.8 ks in 0.1 mol dm^{-3} phosphoric acid electrolyte at 20°C. The resultant anodic films have been characterized using electrochemical impedance spectroscopy, transmission electron microscopy, glow discharge optical emission spectroscopy and Rutherford backscattering spectroscopy. The addition of silicon species to the anodic ZrO_2-WO_3 film significantly enhanced the thermal stability. Even after thermal treatment at 300°C in dry Ar atmosphere, the anodic ZrO_2-WO_3-SiO_2 films revealed stable proton conductivity in the temperature range of 50–225°C, while the anodic ZrO_2-WO_3 on the $Zr_{43}W_{57}$ loses the proton conductivity by annealing at 250°C. The anodic film on the $Zr_{37}W_{47}Si_{16}$ consisted of two layers, comprising an outer thin ZrO_2 layer, free from tungsten and silicon species, and an inner main layer containing all zirconium, tungsten and silicon species. The results in this study suggest that the conductivity deterioration at high annealing temperatures is associated with the diffusion-induced formation of a poorly-conducting layer near the alloy/anodic oxide interface.
© 2011 The Electrochemical Society. [DOI: 10.1149/2.068111jes] All rights reserved.

Manuscript submitted July 8, 2011; revised manuscript received August 15, 2011. Published October 5, 2011.

Anodizing of valve metals, including aluminum, titanium, zirconium, niobium, hafnium and tantalum, leads to formation of barrier-type (compact) or self-organized nanoporous anodic oxide films, depending on the electrolytes used. The oxide films formed are dielectrics or semiconductors with useful properties that make them of great interest for many applications, including solid electrolytic capacitors, solar cells, photocatalysis, electrochromic devices, and self-cleaning materials.[1–5]

It is known that anodic films usually contain hydrogen species,[6] and the authors recently reported that amorphous ZrO_2-WO_3 nanofilms, prepared by anodizing of Zr-50 at% W alloy in phosphoric acid electrolyte, revealed efficient proton conductivity even below 200°C.[7] ZrO_2-WO_3 is an attractive acid catalyst with its Brønsted acidity being comparable to fully anhydrous hydrogen fluoride.[8] As a consequence of its strong acidity, the anodic ZrO_2-WO_3 films may have exhibited the efficient proton conductivity. Such proton-conductive nanofilms are of great interest for application to an electrolyte membrane for intermediate-temperature fuel cells (ITFCs), operating between 100-400°C.[9] The ITFCs have several advantages over polymer electrolyte fuel cells, which operates below 100°C under fully hydrated conditions.[10,11] The fuel cell operation at intermediate temperatures allows the use of non-precious metal electrocatalysts[12] and a range of fuels including hydrocarbons[13] and facilitates simpler module designs compared with high-temperature solid oxide fuel cell.[14] Currently, tailoring of solid electrolytes with high conductivity at intermediate temperatures is a key to develop ITFCs.

Although the authors found the proton-conducting amorphous anodic ZrO_2-WO_3 films with the conductivity being sufficient for fuel cell operation even below 200°C, the thermal stability of the anodic oxide films is low so that the proton conductivity was lost after heating above 200°C. Thus, in the present study, we examined the influence of the addition of silicon species on the proton conductivity of the amorphous anodic ZrO_2-WO_3 films. The anodic ZrO_2-WO_3-SiO_2 films were prepared by anodizing of magnetron-sputtered Zr-47 at% W-16 at% Si (hereafter denoted as $Zr_{37}W_{47}Si_{16}$) in phosphoric acid. The resultant anodic oxide film showed markedly improved thermal stability; even after heating at 300°C, the high proton conductivity was sustained. In the present study, the films were characterized by transmission electron microscopy, glow discharge optical emission spectroscopy and Rutherford backscattering spectroscopy to elucidate the thermal stability and degradation of proton conductivity at higher temperatures.

Experimental

The $Zr_{37}W_{47}Si_{16}$ films, ~350 nm thick, were prepared by DC magnetron sputtering on to flat glass and aluminum substrates. Prior to sputtering, the latter substrates were electropolished and subsequently anodized to provide a flat and smooth surface. The specimens prepared on aluminum substrates were used mostly for characterization of the anodic films by a transmission electron microscope (TEM) and Rutherford backscattering spectroscopy (RBS). The target used for the preparation of the alloy films was 99.9% zirconium disk of 100 mm in diameter with three 99.999% silicon plates (16 × 16 mm) and five 99.99% tungsten discs (20 mm in diameter) located symmetrically on the erosion region. For comparison, silicon-free $Zr_{43}W_{57}$ films were also prepared without placing silicon plates on the target. The compositions of the deposited films were determined using RBS. Then, the deposited films were anodized galvanostatically at a constant current of 10 A m^{-2} up to a selected voltage with current decay for 1.8 ks in a stirred aqueous solution of 0.1 mol dm^{-3} phosphoric acid at 20°C to form anodic films. A platinum sheet was used as a counter electrode.

After depositing a gold bottom electrode of 1 mm diameter, using Hitachi E1030 ion etcher, on the anodic oxide films through a shadow mask to make an alloy film /anodic oxide/Au stack, ionic conductivity was measured by AC impedance spectroscopy. The impedance spectra were measured using a Solartron 1260 frequency response analyzer in a frequency range of 10 to 10^7 Hz at AC amplitude of 20 mV_{rms}. All the measurements were carried out under dry 99.999% argon atmosphere. The dry atmosphere was selected because the proton conductivity of the anodic ZrO_2-WO_3 films was not influenced by the humidity in the atmosphere and showed the stable conductivity even in dry atmosphere.[7] The conductivity was also measured for the specimens that immersed in 0.1 mol dm^{-3} ammonium fluoride solution. The immersion dissolved out an outer ZrO_2 layer, free from tungsten and silicon species, from the anodic films.

Elemental depth profiling analyses of the anodic films were carried out by glow discharge optical emission spectroscopy (GDOES) using a Jobin-Yvon 5000 RF instrument in an argon atmosphere of 600 Pa by applying RF of 13.56 MHz and power of 35 W. The wavelengths of 339.198, 429.461, 288.158, 121.567, 178.287 and 130.217 nm were used for the analysis of zirconium, tungsten, silicon, hydrogen, phosphorus and oxygen, respectively. The signals were detected from a circular area of approximately 4 mm diameter.

* Electrochemical Society Active Member.
z E-mail: habazaki@eng.hokudai.ac.jp

Downloaded 10 Nov 2011 to 133.87.166.192. Redistribution subject to ECS license or copyright; see http://www.ecsdl.org/terms_use.jsp

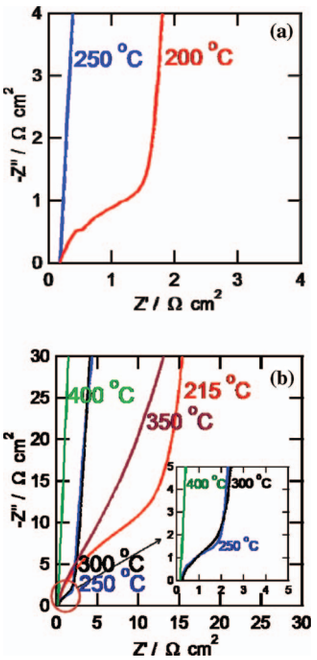

Figure 1. Cole-Cole plots of the impedance spectra of ~200 nm-thick ZrO_2-WO_3 and ZrO_2-WO_3-SiO_2 films measured at 175°C in dry Ar atmosphere. a) The anodic ZrO_2-WO_3 films on the sputter-deposited $Zr_{43}W_{57}$ after post-annealing at 200 and 250°C in dry Ar atmosphere for 1.5 h and b) the anodic ZrO_2-WO_3-SiO_2 films on the sputter-deposited $Zr_{37}W_{47}Si_{16}$ specimens after post-annealing at 215, 250, 300, 350 and 400°C in dry Ar atmosphere for 1.5 h.

Vertical cross-sections of the anodic oxide films were observed using a JEOL JEM-2000FX transmission electron microscope (TEM) operating at 200 kV. The ultrathin cross-sectional specimens were prepared by using a microtome (RMC, MT-7). The compositions of the anodic films and alloy films were determined by RBS, using a 2.0 MeV He^{2+} ion beam supplied by a tandem-type accelerator at Tohoku University. The scattered particles were detected at 170° to the incident beam direction, which was normal to the specimen surface. The data were analyzed using the RUMP program.

Results

It was reported that the anodic ZrO_2-WO_3 films formed on $Zr_{50}W_{50}$ did not show proton conductivity under as-anodized condition.[7] The proton conductivity was activated by post annealing at 200°C. Thus, in this study the anodic ZrO_2-WO_3 films formed on the $Zr_{43}W_{57}$ and the ZrO_2-WO_3-SiO_2 films on the $Zr_{37}W_{47}Si_{16}$ were annealed at several temperatures in dry argon atmosphere for 1.5 h, and then the proton conductivity was measured. The necessity of post-annealing for activation of proton conductivity is the subject of further study. Figure 1 shows the Cole-Cole plots of the impedance spectra of the anodic ZrO_2-WO_3 (Fig. 1a) and ZrO_2-WO_3-SiO_2 (Fig. 1b) films annealed at several temperatures. The ZrO_2-WO_3 film annealed at 200°C reveals a semicircle in the high frequency region and a spike in the low frequency region, which are typical of ionic conductors with blocking electrodes.[14] The spectrum of the anodic film on the present $Zr_{43}W_{57}$ is similar to that on the $Zr_{50}W_{50}$ reported previously.[7] The high frequency semicircle, which is associated with the ionic conduction in the oxide film, disappears after annealing of the silicon-free specimens at 250°C, indicating that the anodic film loses the proton conductivity.

In contrast to the anodic ZrO_2-WO_3 film, the anodic ZrO_2-WO_3-SiO_2 film shows a semicircle at annealing temperatures up to 300°C (Fig. 1b). The high-frequency semicircle becomes smaller at the annealing temperatures of 250 and 300°C than at 215°C. Further increase in the annealing temperature to 350°C enlarges the semicircle and the semicircle disappears completely after annealing at 400°C. It should be worth mentioning here that the conducting species are proton, as confirmed by the change in conductivity in H_2O- and D_2O-containing atmospheres due to the isotope effect.[7] The presence of spike in the low frequency region in Fig. 1 suggests the negligible contribution of electronic conduction in the anodic film.

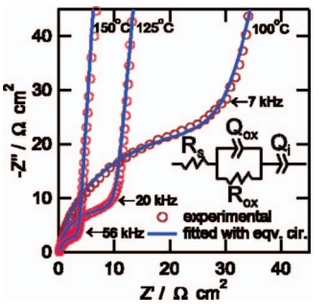

Figure 2. Cole-Cole plots of the impedance spectra of the 200 nm-thick ZrO_2-WO_3-SiO_2 film on the sputter-deposited $Zr_{43}W_{57}$ after post-annealing at 250°C in dry Ar atmosphere for 1.5 h. The impedance spectra were measured at 100, 125, and 150°C in dry Ar atmosphere. The inset shows the equivalent circuit used for the nonlinear least-squares fitting analysis; R_s is the resistance of leads and electrodes, R_{ox} and Q_{ox} are the resistance and capacitance of the film, respectively, and Q_i is a capacitance at the interface between the ion-conductive film and the ion-blocking electrode.

Figure 2 shows the Cole-Cole plots of the anodic ZrO_2-WO_3-SiO_2 film measured at three different temperatures after annealing at 250°C. The high-frequency semicircle becomes smaller at higher temperatures, indicating the increased proton conductivity at higher temperatures. The temperature dependence of the proton conductivity of the ZrO_2-WO_3-SiO_2 films annealed at different temperatures

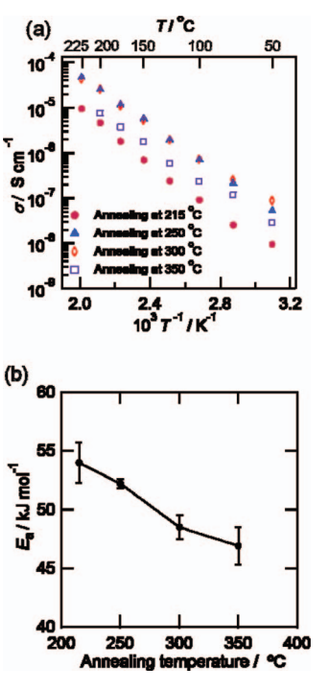

Figure 3. a) Arrhenius plots of proton conductivity, σ, across the ~200 nm-thick ZrO_2-WO_3-SiO_2 films post-annealed at 215, 250, 300 and 350°C in dry Ar atmosphere for 1.5 h and b) activation energy E_a as a function of annealing temperature for the proton conduction. The conductivity was measured in dry Ar atmosphere.

Downloaded 10 Nov 2011 to 133.87.166.192. Redistribution subject to ECS license or copyright; see http://www.ecsdl.org/terms_use.jsp

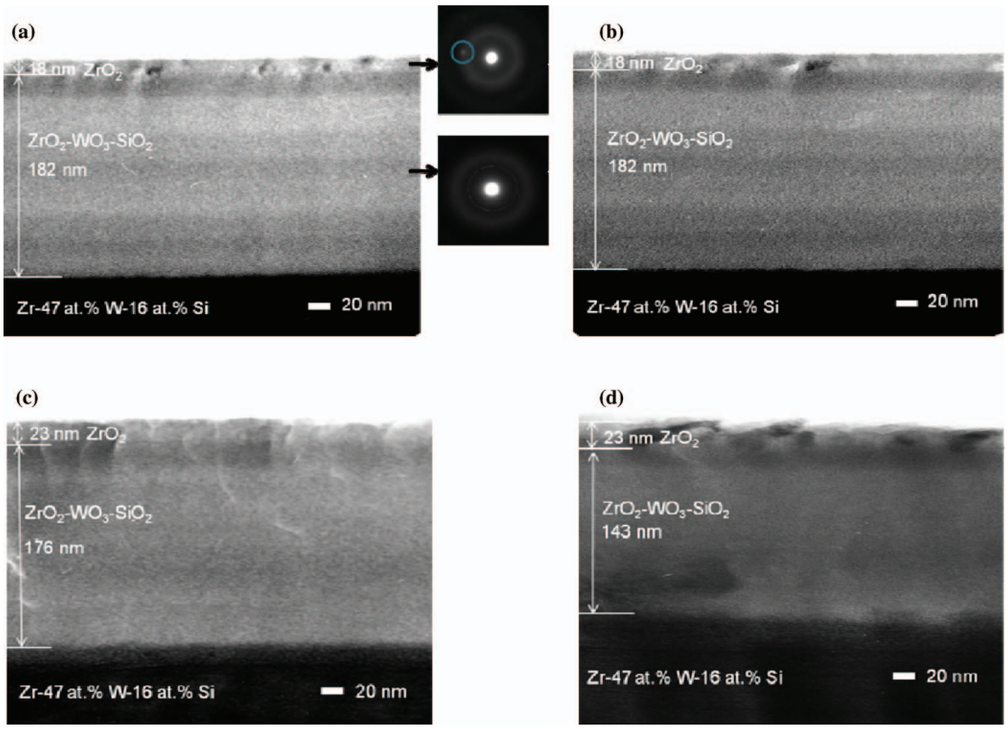

Figure 4. Transmission electron micrographs of ultramicrotomed sections of the ~200 nm-thick anodic films on the sputter-deposited $Zr_{37}W_{47}Si_{16}$ after post-annealing at a) 250°C, b) 300°C, c) 350°C and d) 400°C in dry Ar atmosphere for 1.5 h. Selected area diffraction patterns from the outer and inner layers of the anodic film are also shown in a).

(Fig. 3a) follows Arrhenius behavior. The highest proton conductivity is obtained at each temperature for the specimens annealed at 250 or 300°C. The increase in the annealing temperature from 215 to 250°C increases the conductivity by a factor of five at temperatures above 150°C and by a factor of almost ten at temperatures below 100°C. Thus, the annealing temperature of 215°C is not sufficiently high for the activation of proton conductivity of the ZrO_2-WO_3-SiO_2 film. The conductivities of the ZrO_2-WO_3-SiO_2 film annealed at 250 and 300°C are similar and comparable to those of the ZrO_2-WO_3 film of similar thickness, reported previously.[7] The activation energy is dependent upon the annealing temperature, decreasing with an increase in the annealing temperature (Fig. 3b).

In order to clarify the role of silicon species in improving the thermal stability of the anodic ZrO_2-WO_3 film, the anodized specimens were characterized after annealing at several temperatures. Figure 4 shows TEM images of ultramicrotomed sections of the ZrO_2-WO_3-SiO_2 films after annealing up to 400°C. The ZrO_2-WO_3-SiO_2 film of 200 nm thickness is two layers after annealing at 250°C. The outer layer, 18 nm thick, shows diffraction contrast, suggesting the presence of crystalline oxide. The outer layer is composed of ZrO_2 free from tungsten and silicon species as shown in later GDOES and RBS analyses. The remaining inner layer, 182 nm thick, is apparently featureless, typical of amorphous structure. The amorphous structure is also confirmed from the selected area diffraction pattern shown in Fig. 4a, while the outer layer contains a spot of crystalline oxide. The film structure and the thickness of each layer after annealing at 300°C (Fig. 4b) is the same as that annealed at 250°C. However, the thickness of the outer layer increases to 23 nm, while the remaining inner layer becomes thinner after annealing at 350°C (Fig. 4c). The alloy/anodic oxide interface is also not as sharp as those annealed at and below 300°C. Further increase in the annealing temperature to 400°C reduces markedly the thickness of the anodic film to 166 nm, suggesting the diffusion of oxygen species in the anodic oxide to the alloy film. For the anodic ZrO_2-WO_3 films formed on the silicon-free $Zr_{43}W_{57}$, the film thickness changes from 203 nm to 197 nm by increasing the annealing temperature from 200°C to 250°C (Fig. 5). The

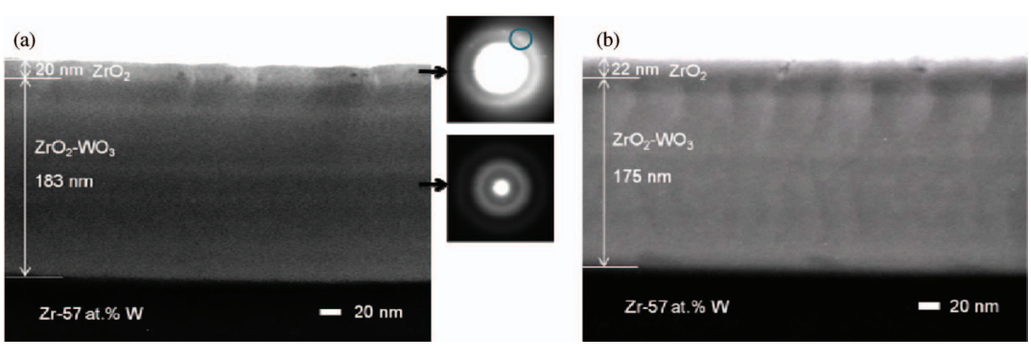

Figure 5. Transmission electron micrographs of ultramicrotomed sections of the ~200 nm-thick anodic films on the sputter-deposited $Zr_{43}W_{57}$ after post-annealing at a) 200°C and b) 250°C in dry Ar atmosphere for 1.5 h. Selected area diffraction patterns from the outer and inner layers of the anodic film are also shown in a).

Downloaded 10 Nov 2011 to 133.87.166.192. Redistribution subject to ECS license or copyright; see http://www.ecsdl.org/terms_use.jsp

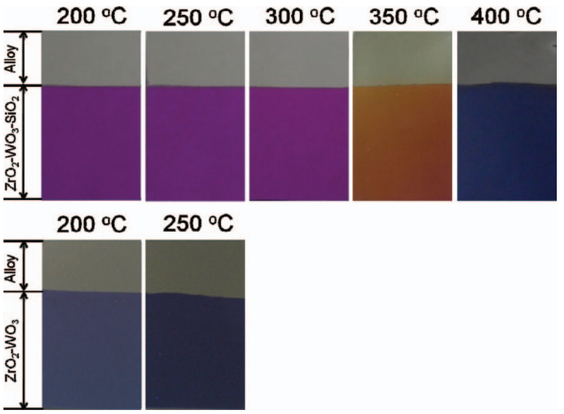

Figure 6. Optical images of the sputter-deposited $Zr_{37}W_{47}Si_{16}$ and $Zr_{43}W_{57}$ specimens anodized at 100 V for 1.8 ks in 0.1 mol dm^{-3} phosphoric acid electrolyte at 20°C to form ~200 nm-thick anodic films and then post-annealed at different temperatures.

alloy/anodic oxide interface and the boundary between the outer layer and the inner layer are unsharpened at the annealing temperature as low as 250°C.

TEM observations revealed the change in the thickness of anodic film with annealing temperature. This was also obvious from the change in the interference color of the specimens. Figure 6 shows the digital camera images of the anodized $Zr_{37}W_{47}Si_{16}$ and $Zr_{43}W_{57}$ specimens after annealing at several temperatures. In agreement with TEM observations, the $Zr_{37}W_{47}Si_{16}$ specimens anodized to 100 V reveal similar purple color up to 300°C and the color change occurs only at and above 350°C. The navy-blue color of the $Zr_{43}W_{57}$ specimen anodized to 100 V becomes darker even at 250°C as a consequence of the change in the film thickness.

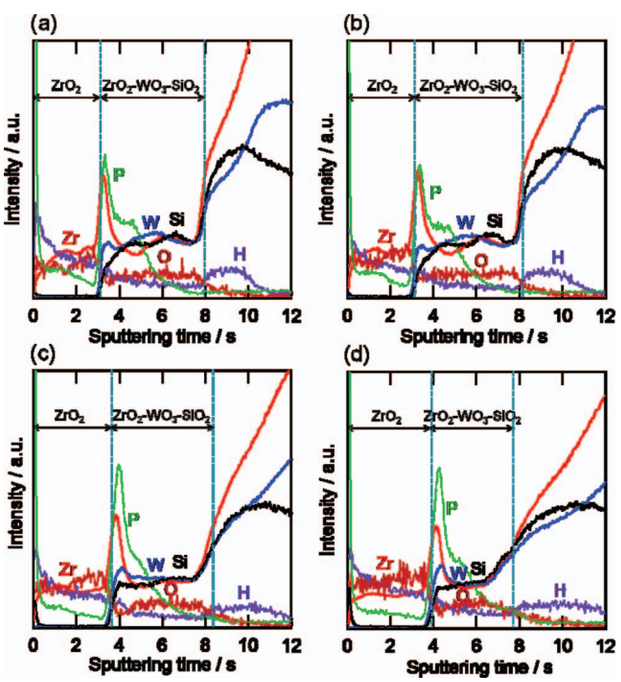

Figure 7. GDOES elemental depth profiles of the ~200 nm-thick anodic films formed on the sputter-deposited $Zr_{37}W_{47}Si_{16}$ at 100 V for 1.8 ks in 0.1 mol dm^{-3} phosphoric acid electrolyte at 20°C and then post-annealed at a) 250°C, b) 300°C, c) 350°C and d) 400°C in dry Ar atmosphere for 1.5 h.

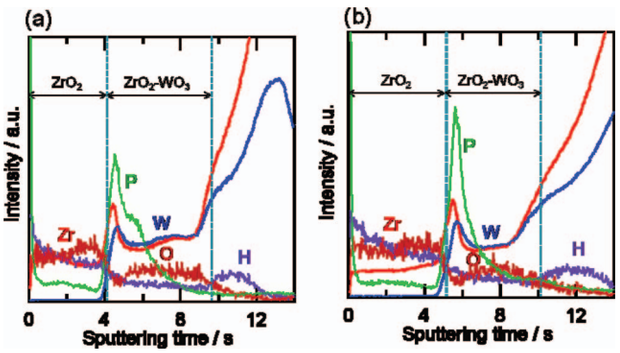

Figure 8. GDOES elemental depth profiles of the ~200 nm-thick anodic films formed on the sputter-deposited $Zr_{43}W_{57}$ at 100 V for 1.8 ks in 0.1 mol dm^{-3} phosphoric acid electrolyte at 20°C and then post-annealed at a) 200°C and b) 250°C in dry Ar atmosphere for 1.5 h.

The elemental depth distributions in the anodic ZrO_2-WO_3-SiO_2 films were examined by GDOES (Fig. 7). The presence of an outer layer practically free from tungsten and silicon species is obvious in the anodic film annealed at 250°C (Fig. 7a). Both tungsten and silicon species are present in the remaining inner layer. Peaks of zirconium and tungsten intensities at the boundary between the inner and outer layers may be artifact, because the enrichment of these species at this boundary region was not detected by RBS analysis as shown later. The ratio of the sputtering time for the outer layer to that for the inner layer is not consistent with their thickness ratio (Fig. 4a), indicating slower sputtering in the outer layer in comparison with the inner layer during depth profile analysis. The phosphorus species are incorporated in the anodic film and distribute to approximately an outer half of the inner layer. Almost similar depth profiles are obtained in the anodic film after annealing at 300°C, but at the annealing temperature of 350°C, the sputtering time for the outer layer is increased and the oxygen diffusion to the alloy film is obvious. These features at 350°C are further enhanced after annealing at 400°C. The alloy/anodic oxide interface of the specimens annealed at 350 and 400°C is also not as sharp as those annealed at 250°C and 300°C. These findings are in agreement with the TEM observations (Fig. 4).

The elemental depth profiles of the anodic ZrO_2-WO_3 film formed on the silicon-free $Zr_{43}W_{57}$ change even at annealing temperature of 250°C (Fig. 8). Unsharpened alloy/anodic oxide interface is obvious after annealing at 250°C.

Precise composition of each layer in the anodic ZrO_2-WO_3-SiO_2 films was obtained by RBS analysis, as listed in Table I. The experimental spectra of the anodic films annealed at 250, 350 and 400°C were replicated well by the simulated spectra obtained using the composition, thickness and density shown in Table I (Fig. 9a). The presence of phosphate anions is neglected in this simulation, because the concentration of phosphate anions in an anodic oxide film is usually ~ 5 at% or less and the atomic scattering factor of phosphorus is much lower than other metal atoms.[7] In agreement with the TEM observation (Fig. 4a), the anodic film annealed at 250°C is two layers, comprising an outer thin ZrO_2 layer free from tungsten and silicon species and an inner layer containing both tungsten and silicon species. The tungsten and silicon are slightly enriched in the inner mixed oxide layer compared with the alloy composition, because a part of zirconium oxidized is used to form an outer layer. The molar ratio of zirconium, tungsten and silicon atoms included in the whole anodic films can be calculated by using thicknesses, densities and compositions given by RBS. In addition, the charge calculated from the number of Zr^{4+}, W^{6+} and Si^{4+} ions in the anodic film annealed at 250°C is in agreement with the charge passed during anodizing. Thus, the anodic film growth proceeds at high current efficiency close to 100% and thermal oxidation during annealing at 250°C is negligible.

Downloaded 10 Nov 2011 to 133.87.166.192. Redistribution subject to ECS license or copyright; see http://www.ecsdl.org/terms_use.jsp

Table I. Results of RBS analysis of the sputter-deposited $Zr_{37}W_{47}Si_{16}$ specimens anodized at 100 V for 1.8 ks in 0.1 mol dm^{-3} phosphoric acid at 20°C and then post-annealed at 250°C, 350°C and 400°C.

Annealing temperature (°C)	Layer	Thickness (nm)	Composition[a]	Oxide density (Mg m^{-3})
	Outer	18	ZrO_2	3.4
250	Inner	182	$(Zr_{0.31}W_{0.50}Si_{0.19})O_{2.50}$	5.0
	Alloy	295	$Zr_{37}W_{47}Si_{16}$	–
	Outer	23	ZrO_2	3.4
	Inner	60	$(Zr_{0.38}W_{0.44}Si_{0.18})O_{2.44}$	4.9
350		116	$(Zr_{0.31}W_{0.50}Si_{0.19})O_{2.50}$	5.0
	Alloy	70	$Zr_{30}W_{38}Si_9\ O_{23}$	–
		221	$Zr_{40}W_{50}Si_{10}$	–
	Outer	23	ZrO_2	3.4
	Inner	100	$(Zr_{0.28}W_{0.50}Si_{0.22})O_{2.50}$	4.9
		43	$(Zr_{0.20}W_{0.50}Si_{0.30})O_{2.30}$	4.9
400	Alloy	95	$Zr_{24}W_{31}Si_{12}\ O_{33}$	–
		30	$Zr_{31}W_{38}Si_{11}\ O_{20}$	–
		90	$Zr_{36}W_{44}Si_{12}\ O_7$	–
		85	$Zr_{39}W_{48}Si_{13}$	–

[a] The presence of phosphorus species was neglected due to relatively low sensitivity and low concentration.[7]

Figure 9b shows the region of the zirconium and tungsten yields of the experimental RBS spectra of the specimens annealed at 250 and 400°C. The leading edge of tungsten shifts slightly to the lower energy after annealing at 400°C, although this is not clear in the energy scale shown in Fig. 9b. The shift is associated with thickening of the outer ZrO_2 layer as shown in Table I. The next sharp increase in tungsten yield appears at higher energy for the specimen annealed at 400°C, suggesting thinning of the anodic film. The yield of zirconium, which is overlapped with tungsten yield, is reduced by increasing the annealing temperature to 400°C, indicating the change in the compositions of the inner layer of the anodic film as well as alloy film. Table I shows oxygen diffusion to the alloy film and the inner layer of the anodic film is divided to two layers with different compositions during annealing at 400°C. Such compositional change due to diffusion at elevated temperatures above 350°C should hinder the proton conductivity.

Discussions

The anodic film formed on the $Zr_{37}W_{47}Si_{16}$ is two layers with an outer thin layer free from tungsten and silicon species, as in the case of the anodic film formed on the $Zr_{50}W_{50}$.[7] The formation of the layered anodic film is associated with the different mobilities of individual species during film growth under the high electric field of $\sim 5 \times 10^8$ V m^{-1}. Although the outer ZrO_2 layer is crystallized after annealing at and above 215°C (Figs. 4 and 5), the anodic films should be amorphous throughout the film thickness before annealing, as found for the film formed on $Zr_{50}W_{50}$.[7] Amorphous anodic oxide is known to grow owing to the simultaneous migration of the anions toward the metal/film interface and cations toward the film/electrolyte interface by a cooperative mechanism so as to form film material both at the metal/film and at the film/electrolyte interfaces.[16] A good correlation between the migration rates of cations and their single metal-oxygen bond energies has been reported.[17–19] The cation species with lower metal-oxygen bond energies migrate faster toward the film/electrolyte interface. The metal-oxygen bond energies decrease in the following order: Si^{4+}-O (465 kJ mol^{-1}) > W^{6+}-O (407 kJ mol^{-1}) > Zr^{4+}-O (276 kJ mol^{-1}). The weakest Zr^{4+}-O bond strength results in the faster migration of zirconium species, forming an outer thin ZrO_2 layer free from tungsten and silicon species. In growing amorphous anodic alumina at high current efficiency, tungsten species migrate slower than aluminum species toward the film/electrolyte interface,[20,21] while silicon species are immobile in various anodic oxides, including anodic aluminum oxide,[22] titanium oxide,[18,23] niobium oxide[24] and tantalum oxide.[1] These facts imply the formation of an intermediate layer containing zirconium and tungsten species, but not silicon species, beneath the outer ZrO_2 layer. However, the intermediate layer was not detected in the present anodic film formed on the $Zr_{37}W_{47}Si_{16}$. In the present anodic film both the tungsten and silicon species are immobile or migrates at the same rate toward the film/electrolyte interface. Assuming that the both tungsten and silicon species are immobile, only the outer ZrO_2 layer is formed at the film/electrolyte interface and the transport number of cations, estimated from the RBS result, is 0.07, which is much smaller than that estimated previously for amorphous anodic ZrO_2.[25] It is, therefore, more likely that both tungsten and silicon species are migrates at a similar rate toward the film/electrolyte interface.

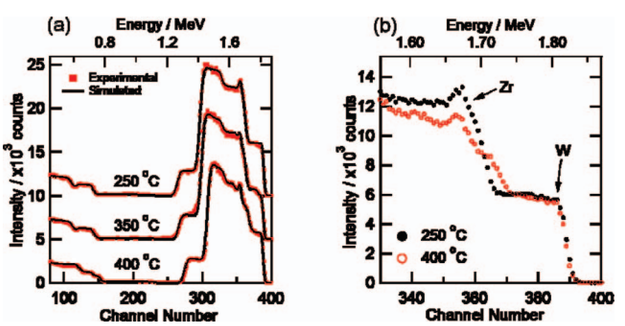

Figure 9. (a) Experimental and simulated RBS spectra for the sputter-deposited $Zr_{37}W_{47}Si_{16}$ specimens anodized at 100 V for 1.8 ks in 0.1 mol dm^{-3} phosphoric acid electrolyte at 20°C and then post-annealed at 250°C, 350°C and 400°C in dry Ar atmosphere for 1.5 h. (b) Enlarged tungsten and zirconium yield region of the experimental RBS spectra for the specimens post-annealed at 250°C and 400°C.

Phosphorus species are incorporated in the anodic film and distribute approximately an outer half of the film thickness. Their distribution suggests their migration toward the alloy/anodic oxide interface at a rate slower than oxygen species.

The authors found previously that the anodic film formed on zirconium did not show proton conductivity.[7] Thus, the outer ZrO_2 layer should not be an efficient proton-conducting layer. In fact, the removal of the outer ZrO_2 layer from the 180 nm-thick ZrO_2-WO_3 film formed on the $Zr_{50}W_{50}$ increased the proton conductivity by almost one order of magnitude.[7] In the present study, the outer ZrO_2 layer thickens and the proton conductivity is lost or deteriorated after annealing at 250°C for the anodic ZrO_2-WO_3 film and at and above 350°C for the anodic

Downloaded 10 Nov 2011 to 133.87.166.192. Redistribution subject to ECS license or copyright; see http://www.ecsdl.org/terms_use.jsp

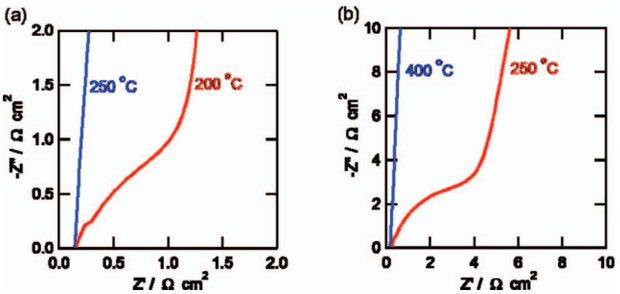

Figure 10. Cole-Cole plots of the impedance spectra of ~180 nm-thick (a) ZrO_2-WO_3 and (b) ZrO_2-WO_3-SiO_2 anodic films without the outer ZrO_2 layer, measured at 125°C in dry Ar atmosphere. The outer layer was removed by immersing the anodized specimens in 0.1 mol dm^{-3} ammonium fluoride solution after annealing at the temperatures at a) 200°C and 250°C and b) 250°C and 400°C.

ZrO_2-WO_3-SiO_2 film. In order to know if thickening of the outer layer has a major role in such deterioration of proton conductivity, the outer layer was removed chemically by immersing in a fluoride-containing solution after annealing of the anodized $Zr_{43}W_{57}$ and $Zr_{37}W_{47}Si_{16}$ at selected temperatures. The complete removal of the outer layer from each specimen was confirmed by GDOES elemental depth profile analysis. Figure 10 shows the Cole-Cole plots of the impedance spectra of the anodic ZrO_2-WO_3 (Fig. 10a) and ZrO_2-WO_3-SiO_2 (Fig. 10b) films without an outer layer, measured at 125°C. Even after removing the outer layer no semicircle appears for the ZrO_2-WO_3 specimen annealed at 250°C and ZrO_2-WO_3-SiO_2 specimen annealed at 400°C. Thus, the deterioration of the proton conductivity is not caused by the thickening of the outer layer. For the specimens post-annealed at appropriate temperatures, the removal of the outer layer increased the proton conductivity. Further detailed study on the role of the outer layer will be reported in a separate paper.

GDOES elemental depth profiles shown in Figs. 7 and 8 reveal the presence of hydrogen species. The hydrogen species are present even after annealing at 400°C and their distributions are not influenced by changing the annealing temperature. Thus, even though protons are present, the proton conductivity is deteriorated at higher annealing temperatures. When obvious diffusion of oxygen from the anodic film to the alloy film occurs, the proton conductivity is deteriorated. Such diffusion changes the film composition as well as thickness, probably causing the degradation of proton conductivity. The presence of silicon in the anodic film and alloy film suppress the diffusion, improving the thermal stability.

Conclusions

Amorphous anodic ZrO_2-WO_3-SiO_2 nanofilms as well as ZrO_2-WO_3 nanofilms are a new class of proton-conducting electrolyte that has the efficient conductivity in the intermediate temperature range. The deterioration of proton conductivity of the anodic films is involved by the formation of the diffusion-induced poorly-conducting layer probably near the alloy/anodic oxide interface during post-annealing at elevated temperatures. The diffusion during post-annealing is clearly suppressed by silicon addition into the Zr-W system. As a result, anodic ZrO_2-WO_3-SiO_2 films can retain the high proton conductivity even after annealing at 300°C whereas the anodic ZrO_2-WO_3 loses the conductivity at around 200°C. Various complex oxides with strong Brønsted acidity and thermal tolerance can be fabricated readily by a combination of alloy deposition by physical vapor deposition (PVD) and anodizing of the deposited material; such oxides show high potential as efficient proton conductors. The current results strongly suggest that the anodic oxidation poses strong technique to design the proton conducting oxide membrane.

Acknowledgments

The present work was supported in part by the Global COE Program (Project No. B01: Catalysis as the Basis for Innovation in Materials Science) from the Ministry of Education, Culture, Sports, Science and Technology, Japan, a Grant-in-Aid for Exploratory Research, No. 23656441 from the Japan Society for the Promotion of Science, and the Asahi Glass Foundation.

References

1. K. Shimizu, K. Kobayashi, G. E. Thompson, P. Skeldon, and G. C. Wood, *Philos. Mag. B*, **73**, 461 (1996).
2. K. Tsujii, T. Yamamoto, T. Onda, and S. Shibuichi, *Angew. Chem. Int. Ed.*, **36**, 1011 (1997).
3. H. Habazaki, K. Shimizu, S. Nagata, K. Asami, K. Takayama, Y. Oda, P. Skeldon, and G. E. Thompson, *Thin Solid Films*, **479**, 144 (2005).
4. E. Balaur, J. M. Macak, L. Taveira, and P. Schmuki, *Electrochem. Commun.*, **7**, 1066 (2005).
5. C. A. Grimes, *J. Mater. Chem.*, **17**, 1451 (2007).
6. L. Iglesias-Rubianes, P. Skeldon, G. E. Thompson, U. Kreissig, D. Grambole, H. Habazaki, and K. Shimizu, *Thin Solid Films*, **424**, 201 (2003).
7. D. Kowalski, Y. Aoki, and H. Habazaki, *Angew. Chem. Int. Ed.*, **48**, 7582 (2009).
8. G. Busca, *Chem. Rev.*, **107**, 5366 (2007).
9. T. Norby, *Solid State Ionics*, **125**, 1 (1999).
10. K. Schmidt-Rohr and Q. Chen, *Nat. Mater.*, **7**, 75 (2008).
11. O. Diat and G. Gebel, *Nat. Mater.*, **7**, 13 (2008).
12. P. Heo, M. Nagao, M. Sano, and T. Hibino, *J. Electrochem. Soc.*, **154**, B53 (2007).
13. P. Heo, K. Ito, A. Tomita, and T. Hibino, *Angew. Chem. Int. Ed.*, **47**, 7841 (2008).
14. M. Nagao, M. Takahashi, and T. Hibino, *Energy Environ. Sci.*, **3**, 1934 (2010).
15. J. T. S. Irvine, D. C. Sinclair, and A. R. West, *Adv. Mater.*, **2**, 132 (1990).
16. J. P. S. Pringle, *Electrochim. Acta*, **25**, 1423 (1980).
17. H. Habazaki, K. Shimizu, P. Skeldon, G. E. Thompson, and G. C. Wood, *J. Surf. Finish. Soc. Jpn.*, **49**, 854 (1998).
18. H. Habazaki, K. Shimizu, S. Nagata, P. Skeldon, G. E. Thompson, and G. C. Wood, *J. Electrochem. Soc.*, **149**, B70 (2002).
19. S. Koyama, Y. Aoki, S. Nagata, H. Kimura, and H. Habazaki, *Electrochim. Acta*, **55**, 3144 (2010).
20. K. Shimizu and K. Kobayashi, *J. Surf. Finish. Soc. Jpn.*, **46**, 402 (1995).
21. H. Habazaki, K. Shimizu, P. Skeldon, G. E. Thompson, and G. C. Wood, *Philos. Mag. B*, **73**, 445 (1996).
22. G. C. Wood, P. Skeldon, G. E. Thompson, and K. Shimizu, *J. Electrochem. Soc.*, **143**, 74 (1996).
23. H. Habazaki, K. Shimizu, S. Nagata, P. Skeldon, G. E. Thompson, and G. C. Wood, *Corros. Sci.*, **44**, 1047 (2002).
24. H. Habazaki, T. Matsuo, H. Konno, K. Shimizu, S. Nagata, K. Matsumoto, K. Takayama, Y. Oda, P. Skeldon, and G. E. Thompson, *Electrochim. Acta*, **48**, 3519 (2003).
25. H. Habazaki, M. Uozumi, H. Konno, K. Shimizu, S. Nagata, K. Asami, K. Matsumoto, K. Takayama, Y. Oda, P. Skeldon, and G. E. Thompson, *Electrochim. Acta*, **48**, 3257 (2003).

Downloaded 10 Nov 2011 to 133.87.166.192. Redistribution subject to ECS license or copyright; see http://www.ecsdl.org/terms_use.jsp